IOP Conf. Series: Materials Science and Engineering **63** (2014) 012117 doi:10.1088/1757-899X/63/1/012117

High strength and high electrical conductivity of UFG Al-2%Fe alloy achieved by high-pressure torsion and aging

J M Cubero-Sesin[1,2], M Arita[1], M Watanabe[3] and Z Horita[1,2]
[1]Department of Materials Science and Engineering, Kyushu University, Fukuoka, Japan 819-0395
[2]WPI, International Institute for Carbon-Neutral Energy Research (WPI-I2CNER), Kyushu University
[3]Department of Materials Science and Engineering, Lehigh University, Bethlehem, PA, 18015
E-mail: cubero@zaiko6.zaiko.kyushu-u.ac.jp

Abstract. In this study, Al-2%Fe samples extracted from a cast ingot in the shape of rings were processed by High-Pressure Torsion (HPT) at room temperature. Suitable specimens were extracted for evaluation of mechanical properties and electrical resistivity. High tensile strength of ~600 MPa was attained by HPT due to grain refinement down to an average grain size of ~130 nm and by subsequent aging accompanied by nano-sized (~10 nm) Al_6Fe precipitates. The resulting conductivity (IACS%) was recovered from ~40% in the steady state after HPT to well above 50% in the peak-aged condition, which is in the range of current Al electrical alloys.

Keywords: *aluminum alloys, ultrafine grains, high strength, electrical conductivity*

1. Introduction

Al alloys have become very important materials not only due to the high specific strength with lower density, but also due to their good electrical conductivity [1, 2]. For this purpose, insoluble alloying elements such as Fe are preferred since they are less harmful as a form of intermetallic compounds than in solid solution [2]. In this study, High-Pressure Torsion (HPT) [3] was used to control microstructures of Fe-containing phases in Al-Fe alloys in conjunction with an aging treatment, in order to improve not only the strength and ductility but also their electrical conductivity. An optimal combination of high strength with good ductility was achieved by room-temperature HPT processing of disk samples from a cast Al-2%Fe alloy, as shown in a previous report [4]. HPT processing under equivalent conditions was carried out on ring-shaped samples [5], in order to extract specimens suitable for evaluation of electrical conductivity. The effect on the electrical conductivity of both the imposed strain by HPT and recovery by subsequent aging treatments was evaluated. The goal of this paper was to demonstrate that high electrical conductivity can be obtained without sacrificing the strength by aging after HPT, which creates precipitation of the supersaturated Fe content in the matrix and recovery of the defects created by the HPT processing, towards the applicability of this alloy for fabrication of electrical conductors.

2. Experimental Procedures

Samples in the form of rings with 20mm outer diameter and 3mm width were extracted from an Al-2%Fe cast alloy, with initial thicknesses of 0.9 ± 0.1 mm and processed by HPT under an applied pressure of 3 GPa. Processing was performed at room temperature for up to N=30 revolutions using a rotation speed of 1 rpm. The final thickness after HPT was of 0.6 ± 0.1 mm. Measurements of Vickers microhardness were carried out on the surfaces of the rings, along 12 radial directions with 0.5mm spacing before and after aging treatments at 200°C and quenching in ice water. Fig. 1 shows a schematic of the HPT ring and the dimensions of the extractions used for measurements of electrical conductivity. The electrical conductivity was measured using a 4-point circuit (to a maximum current of ±300 mA) through

specimens with a cross-section of 0.3 x 0.3 mm² and a probe separation of 17.8 mm. The location of the voltage and current probes is also indicated in Fig. 1. In addition, 3mm diameter disks were punched from the rings, ground to 0.15 mm and further thinned by twin-jet electropolishing in a solution of 20% sulfuric acid in methanol for observation by high-resolution scanning transmission electron microscopy (HRSTEM). X-ray diffraction (XRD) analysis was conducted to identify intermetallic phases present in the alloy.

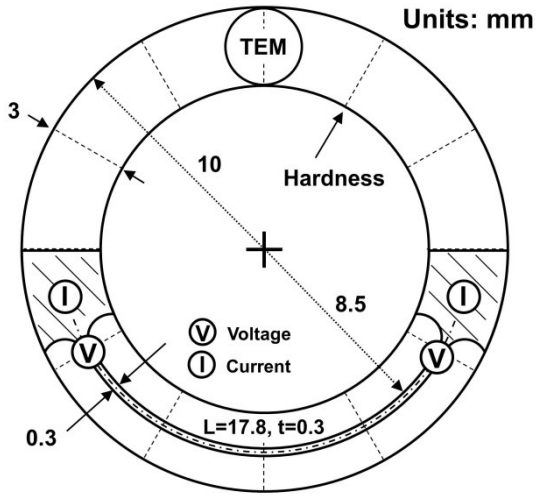

Fig. 1. Schematic of HPT ring and specimen for measurement of electrical resistivity

3. Results and Discussion

3.1. The initial microstructure

XRD analysis confirmed that as a result of the effective cooling rate in the casting process, two eutectic phases were present in the as-cast condition: metastable Al+Al_6Fe and stable Al+Al_3Fe. The alloy was annealed at 500 °C for 1 h and cooled in the furnace to minimize Fe content in the Al matrix to an equilibrium value (~0.05%). The microstructure examined by optical microscopy after annealing is shown in Fig. 2. The dendritic type α-Al is observed surrounded by eutectic phases, as expected from the Al-Fe phase diagram [6]. As a result of the annealing, no significant coarsening of the microstructure occurred, but precipitation of small particles within the α-Al dendrites, as well as small changes in the morphology of the eutectic phases were observed. The Al_3Fe can be seen in Fig. 2 as coarser lamellae with a width of ~1.5 μm, particularly at dendrite and cell boundaries. The Al_6Fe composes fine fibers with diameters ranging from 150-200 nm, arranged in cellular structures.

3.2. Microstructure observations after HPT processing

TEM observations of the microstructure after HPT processing are shown in Fig. 3(a) for N=1 and in Fig. 3(b) for N=10. The microstructure after N=1 is composed mostly of an equiaxed and submicron-sized grain structure, but some heterogeneity develops as a result of deformation around the hard eutectic particles. As a result, regions with dislocation substructures can be seen in Fig. 3(a), whereas no such substructures are observed in the corresponding image in Fig. 3(b). Inspection of several areas by TEM showed that the original eutectic structures could be distinguished in a few limited areas after N=1 but no trace of them could be identified after N=10. Inspection of the corresponding selected-area

electron diffraction (SAED) patterns shows that the grain size decreases and the grain misorientation increased with HPT processing through N=10, as a ring-like pattern forms in Fig. 3(b) but a net pattern forms in Fig. 3(a). The grain size is measured to be ~550 nm after N=1 and ~130 nm after N=10, which is consistent with the grain size reported in [4].

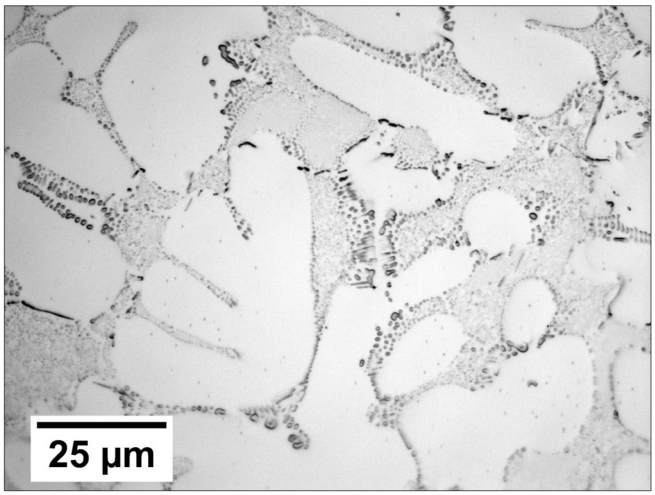

Fig. 2. Microstructure of cast Al-2%Fe after annealing at 500 °C for 1 h

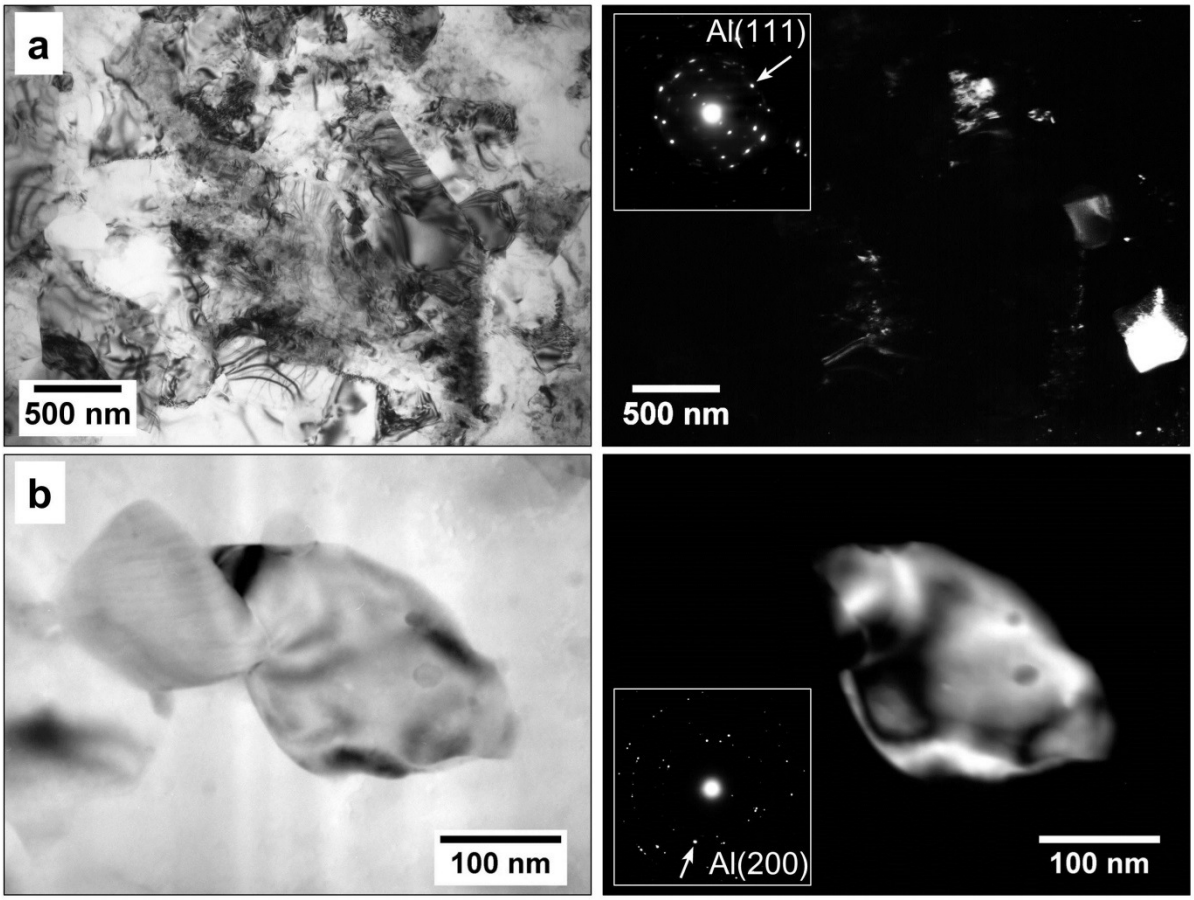

Fig. 3. TEM bright-field (left) and dark-field images (right) showing microstructure after HPT processing through (a) N=1 and (b) N=10 revolutions. Dark-field images obtained from selected beams as pointed by arrows in corresponding SAED patters (as insets)

3.3. Microstructures after aging

STEM observations were performed both in a bright-field (BF) mode and a high-angle annular dark-field (HAADF) mode, in samples processed through the same level of imposed strain for the as-HPT condition and the peak hardness condition in order to compare their microstructures. The BF image in Fig. 4(a) shows that an ultrafine-grained structure was attained by HPT in accordance with the observations by dark-field TEM. Fig. 4(b) shows that the structure maintained the fine-grained condition after aging at 200 °C for 0.5 h to peak hardness. The HAADF image in Fig. 4(b) shows a fine distribution of particles in bright contrast, when compared to the image in Fig. 4(a). The particles A and B, as indicated by arrows in the HAADF image of Fig. 4(b) were analyzed by EDS and their corresponding spectra are shown in Fig. 4(c). The particles of bright contrast were confirmed to be Fe-rich. The peaks of Cu and Cr are due to interactions of the electron beam with the sample holder and the instrument column, respectively. It was reported earlier [4] that supersaturation of Fe occurred to ~0.5%Fe in this sample along with fragmentation and dispersion of the original eutectic particles. It is suggested from Fig. 4(b) that nano-sized particles precipitated during aging in the Al matrix with Fe supersaturated by HPT processing.

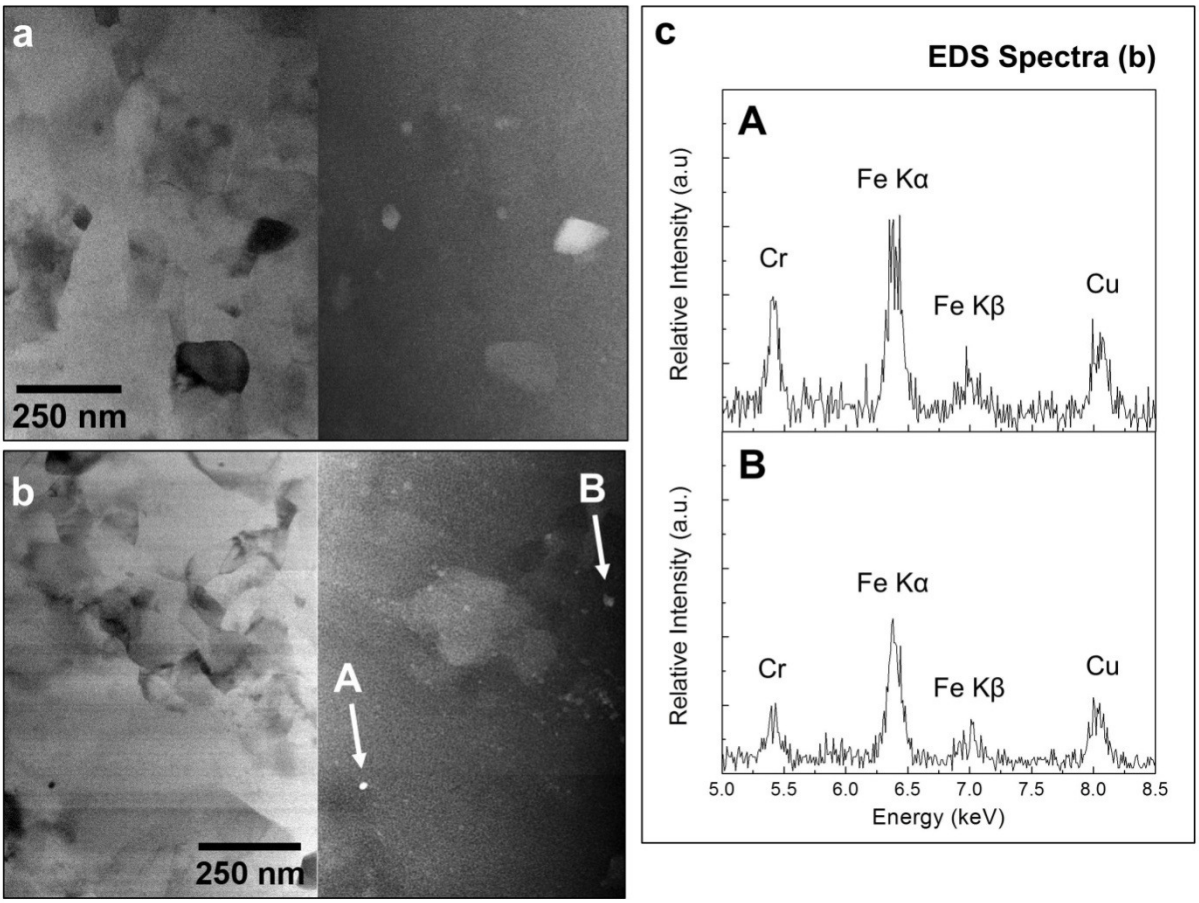

Fig. 4. STEM bright-field (left) and HAADF images (right) from samples processed by HPT through (a) N=10 revolutions and (b) N=10 revolutions and aged at 200 °C for 0.5 h (peak-aged). EDS spectra in (c) obtained from A and B as indicated by corresponding arrows in (b)

Fig. 5(a) shows an HRTEM image from the sample processed by HPT through N=10 revolutions and subsequently aged at 200 °C to the peak condition, presenting a particle in dark contrast with a size of ~5 nm within a grain with a size of ~100 nm. The lattice image from the region enclosed by the dotted line in Fig. 5(a) is enlarged in Fig. 5(b). The Fast Fourier Transform (FFT) analysis of the region in the inset image of Fig. 5(b) indicates that it corresponds to Al_6Fe. The diffraction spots circled in the diffraction pattern shown in Fig. 5(c) correspond to the (223) lattice planes in the orthorhombic structure and indicate that this plane is parallel to the (002) matrix planes. Several dislocations in the (002) lattice planes exist around the particle to accommodate the misfit as marked 'T' in Fig. 5(b). From the analysis reported earlier [7], it is stated that a semi-coherent Al_6Fe phase is dominant for the precipitation from the solid solution. The size of these particles is similar to the one in bright contrast in Fig. 4(b), which indicates that the HPT processing accelerates aging for the precipitation in this alloy.

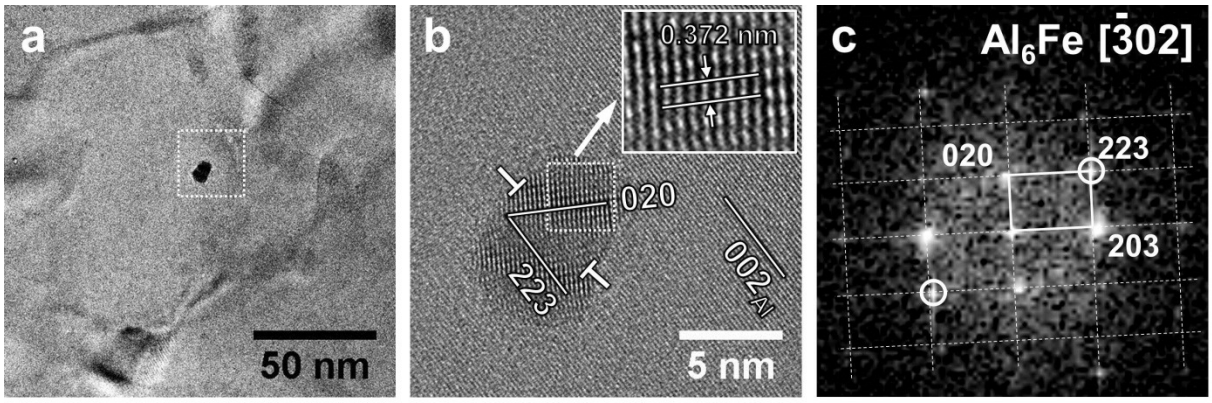

Fig. 5. (a) HRTEM image from sample processed by HPT through N=10 revolutions and aged at 200 °C for 0.5 h (peak-aged). Lattice image in (b) obtained from region in dotted line in (a). Diffraction pattern shown in (c) obtained by FFT from region in inset in (b)

3.4. Mechanical properties

Fig. 6 plots Vickers microhardness against the distance from the ring center for samples processed by HPT through different numbers of revolutions and after aging to peak hardness. Microhardness is relatively homogeneous across the radius of the rings, which is an advantage of the ring HPT process [5]. In HPT, the following expression is used to estimate the equivalent strain [3],

$$\varepsilon_{HPT} = \frac{2\pi rN}{\sqrt{3}t} \quad (1)$$

where N is the number of revolutions, r is the distance from the ring center and t is the thickness of the rings after HPT processing. A strain gradient of hardness with respect to the distance from the ring center is not observed after N=0.5 or 1, but a gradient at higher numbers of revolutions can be observed, especially if the measurement at r=7.5 mm is excluded, since the ring is slightly thinner at the inner edge. Hardness increases with

increasing the number of revolutions to a steady-state level of ~175 HV after N=30. Age hardening was achieved consistently in samples processed through N=0.5, 5 and 30 within 0.5 h of aging at 200 °C to reach ~200 HV for the latter sample. Thus time to reach the peak-aged condition was similar regardless of the number of revolutions. The hardness starts to decrease from the peak-aged condition after 8 h of aging in the samples processed through N=30.

Fig. 7 shows the microhardness data plotted against the equivalent strain calculated using Eq. 1. The result shows that the hardness increase is a unique function of equivalent strain, which is consistent with the previous reports for disk samples [4, 6]. This allows us to correlate with the results of the tensile tests after HPT processing and after aging. Table 1 summarizes the results of tensile tests from specimens extracted from disk samples processed at equivalent levels of imposed strain as the ring samples. Very high strength was achieved by HPT processing with good ductility. Strength increases in the peak-aged condition but at the expense of some uniform elongation, possibly due to stress concentration in regions with a high density of precipitates.

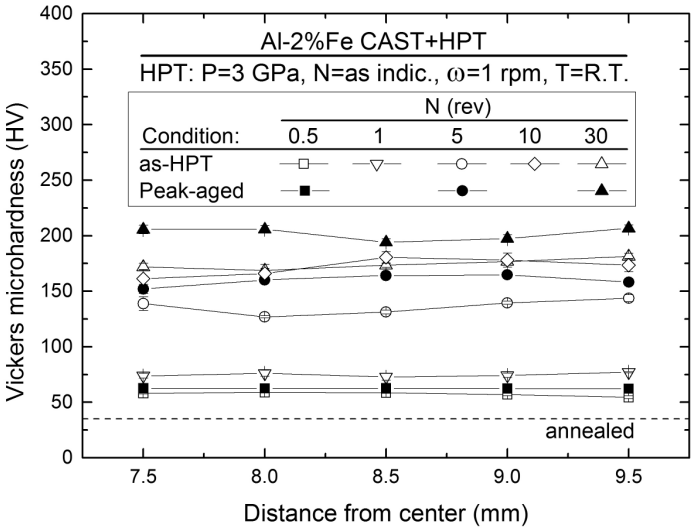

Fig. 6. Vickers microhardness (HV) as function of distance from ring center

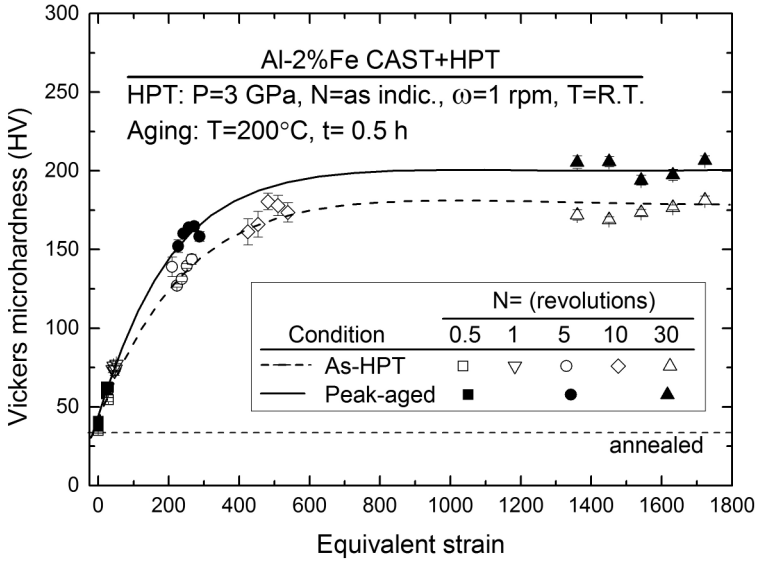

Fig. 7. Vickers microhardness (HV) as function of equivalent strain

3.5. Electrical conductivity measurements

Table 1 also includes the results of electrical conductivity from the ring samples. The resulting conductivity values (IACS%) from samples in the as-HPT condition decrease with respect to the equivalent strain and saturate to ~40% in a way similar to the trend shown in Fig. 7. However, after aging the samples to peak-hardness, the electrical conductivity is recovered to ~55% and ~53% in the samples processed for 5 and 30 revolutions, respectively. These values of conductivity can be classified in the range of current Al electrical alloys [2], but this alloy shows superior strength with good uniform and total elongation. Both recovery of microstructure and precipitation of dissolved Fe aid to improve the electrical conductivity. The high strength can be maintained by age hardening achieved by the coherency strains of the precipitates and also the stability of the ultrafine-grained microstructure up to the peak hardness condition. Therefore, a simultaneous increase of strength and electrical conductivity can be achieved by combination of HPT processing and proper aging treatment.

Table 1. Summary of tensile test and electrical conductivity results

		As-HPT				**Peak-aged (T=200°C; t=0.5 h)**			
N [rev]	ε_{strain}	UTS [MPa]	$\varepsilon_{uniform}$ [%]	ε_{total} [%]	IACS% [±5%]	UTS [MPa]	$\varepsilon_{uniform}$ [%]	ε_{total} [%]	IACS% [±5%]
0 (annealed)	0	120	35	53	56	-	-	-	-
0.5	25	-	-	-	55	-	-	-	66
5	250	535	11	18	41	610	6	9	55
30	1500	620	5	9	40	650	3	8	53

4. Summary and Conclusions

High strength as ~ 600 MPa UTS was attained by HPT processing of an Al-2%Fe alloy due to the formation of an ultrafine-grained structure as well as dispersion and partial dissolution of Fe-containing phases. Subsequent aging at 200°C show that precipitation hardening was achieved accordingly to increase the tensile strength well above 600 MPa as well as significant recovery of electrical conductivity to well over 50 IACS%. The results presented in this work demonstrate large potential for application of the alloy as a high strength, lightweight electrical conductor.

Acknowledgements

This study was carried out as a part of a materials development program in the Japan Aluminum Association. The authors would like to recognize Dr. Q. He and Mr. A. Wade in Lehigh University for their cooperation with the electron microscopy. One of the authors (JC) thanks the Ministry of Education, Culture, Sports, Science and Technology (MEXT) of Japan for a PhD scholarship. This work was supported in part by Japan Science and Technology Agency (JST) under Collaborative Research Based on Industrial Demand “Heterogeneous Structure Control: Towards Innovative Development of Metallic Structural Materials”, in part by the Light Metals Educational Foundation of Japan and in part by a Grant-in-Aid for Scientific Research from the Ministry of Education, Culture, Sports, Science and Technology of Japan in the Innovative Area "Bulk Nanostructured Metals"(22102004).

References

[1] Totten G E and MacKenzie D S 2003 *Handbook of Aluminum vol 2: Alloy Production and Materials Manufacturing* (New York, NY: Marcel Dekker, Inc.)
[2] Bray J W 1992 *ASM Handbook vol 2 - Properties and Selection: Nonferrous Alloys and Special-Purpose Materials* (Metals Park, OH: ASM International)
[3] Valiev R Z, Estrin Y, Horita Z, Langdon T G, Zehetbauer M J and Zhu Y T 2006 *JOM* **58** 33
[4] Cubero-Sesin J M and Horita Z 2013 *J. Mater. Sci.* **48** 4713
[5] Harai Y, Ito Y and Horita Z 2008 *Scripta Mater.* **58** 469
[6] Kattner U R and Burton B P 1992 ASM Handbook vol 3 - Alloy Phase Diagrams (Metals Park, OH: ASM International) p 2-44
[7] Cubero-Sesin J M and Horita Z 2013 *Proceedings of the 8th Pacific Rim International Conference on Advanced Materials and Processing (PRICM-8)* (Waikoloa, HI) ISBN: 978-0-470-94309-0 (New York, NY: Wiley) p 3323